Ocean Sci. Discuss., 11, 2289–2335, 2014
www.ocean-sci-discuss.net/11/2289/2014/
doi:10.5194/osd-11-2289-2014

Ocean Science
Discussions
Open Access

Transient tracer applications in the Southern Ocean

T. Stöven[1], T. Tanhua[1], and M. Hoppema[2]

[1]Helmholtz Centre for Ocean Research Kiel, GEOMAR, Germany
[2]Alfred Wegener Institute Helmholtz Centre for Polar and Marine Research, Bremerhaven, Germany

Received: 18 August 2014 – Accepted: 15 September 2014 – Published: 16 October 2014

Correspondence to: T. Stöven (tstoeven@geomar.de)

Published by Copernicus Publications on behalf of the European Geosciences Union.

Abstract

Transient tracers can be used to constrain the Inverse-Gaussian transit time distribution (IG-TTD) and thus provide information about ocean ventilation. Individual transient tracers have different time and application ranges which are defined by their atmospheric history (chronological transient tracers) or their decay rate (radioactive transient tracers). The classification ranges from tracers for highly ventilated water masses, e.g. sulfur hexafluoride (SF_6), the decay of Tritium (δ^3H) and to some extent also dichlorodifluoromethane (CFC-12) to tracers for less ventilated deep ocean basins, e.g. CFC-12, Argon-39 (^{39}Ar) and radiocarbon (^{14}C). The IG-TTD can be empirically constrained by using transient tracer couples with sufficiently different input functions. Each tracer couple has specific characteristics which influence the application limit of the IG-TTD. Here we provide an overview of commonly used transient tracer couples and their validity areas within the IG-TTD by using the concept of tracer age differences (TAD).

New measured CFC-12 and SF_6 data from a section along 10° E in the Southern Ocean in 2012 are presented. These are combined with a similar data set of 1998 along 6° E in the Southern Ocean as well as with ^{39}Ar data from the early 1980s in the western Atlantic Ocean and the Weddell Sea for investigating the application limit of the IG-TTD and to analyze changes in ventilation in the Southern Ocean. We found that the IG-TTD can be constrained south to 46° S which corresponds to the Subantarctic Front (SAF) denoting the application limit. The constrained IG-TTD north of the SAF shows a slight increase in mean ages between 1998 and 2012 in the upper 1200 m between 42–46° S. The absence of SF_6 inhibits ventilation analyses below this depth. The time lag analysis between the 1998 and 2012 data shows an increase in ventilation down to 1000 m and a steady ventilation between 2000 m-bottom south of the SAF between 51–55° S.

1 Introduction

Ocean ventilation plays a major role in climate. It affects transport processes from the surface into the ocean's interior and vice versa, carrying dissolved gases, nutrients, microorganisms but also soluble hazardous substances and other coastal and offshore pollutions (Schlosser et al., 1999). One of the most prominent processes is the accumulative uptake of anthropogenic carbon (C_{ant}) at high and mid latitudes, where large volumes of surface and intermediate waters are transported into deeper water layers (Sabine and Tanhua, 2010). The uptake of atmospheric carbon dioxide (CO_2) by the ocean influences the marine ecology and biology, e.g. inhibiting shell building marine organisms due to acidification (Orr et al., 2005). With focus on the economically important marine resources like fish and seafood, the oxygen supply by ventilation represents another field of interest. To this end, ocean ventilation models are an important part of describing and understanding the complex biogeochemical interactions in the ocean.

A well-established concept is the transit time distribution (TTD) model which provides information about ventilation timescales and rates (Hall and Plumb, 1994; Bolin and Rodhe, 1973). The TTD model has several solutions and intended application possibilities. For example, the one dimensional Inverse-Gaussian transit time distribution (IG-TTD) can be applied to field data of transient tracer surveys in the ocean (Waugh et al., 2003). An IG-TTD can be empirically constrained with a transient tracer couple which provides reliable mean age results of water masses in the ocean (Stöven and Tanhua, 2014). However, the used tracers of a couple have different influences on the limits of the IG-TTD, i.e. different validity areas, so that every tracer couple is restricted to a specific application range. Furthermore, the IG-TTD model is not only limited by the used tracer couples, but also by different ventilation structures which do not necessarily correspond to the assumptions of the IG-TTD. Possible applicabilities of the IG-TTD are usually investigated by trial and error which can be very time consuming.

Here we present an overview of some commonly used transient tracers and their current and future specific restrictions of use with the IG-TTD. Section 2 highlights

Discussion Paper | Discussion Paper | Discussion Paper | Discussion Paper |

OSD

11, 2289–2335, 2014

Tracers in the Southern Ocean

T. Stöven et al.

the power and weaknesses of each transient tracer with focus on the analytical and natural limits as well as other special features. Section 3 includes mean age matrices of the IG-TTD, which are shown to indicate the different time ranges of the transient tracers. Furthermore, a new method is introduced which allows for a fast and simple classification of the applicability of the IG-TTD to certain field data and which also describes the validity areas of the tracer couples. In Sect. 4 data sets from two transient tracer surveys in the Southern Ocean are presented. The transient tracer structure and changes in ventilation were analyzed using the IG-TTD. Hereby, the new method was applied to determine the limits of the IG-TTD and the corresponding tracers. Possible solutions of the determined restrictions are shown, e.g. the use of argon data in deep water. This work should serve as extension of the work by Stöven and Tanhua (2014) with the main focus on the future scope of IG-TTD applications.

2 Transient tracers

2.1 Sulfur hexafluoride

Sulfur hexafluoride (SF_6) is an inorganic compound which was first synthesized in the beginning of the 20th century. It is produced since the early 1950s in an industrial-scale, mainly as insulating and quenching gas for high voltage systems. The atmospheric sources are thereby restricted to non-natural emissions by industrial plants. It is a highly inert gas with a very low degradation rate by UV radiation leading to an atmospheric lifetime of up to 3200 yr (Ravishankara et al., 1993). Significant sinks besides the ocean uptake are unknown or negligible. The concentration is stated in ppt which is independent of temperature and salinity. The current concentration in the atmosphere is ≈ 8 ppt in 2014 and still increasing with a stable emission rate. The use of SF_6 as a transient tracer in the ocean is restricted in less ventilated water masses where concentrations are below the detection limit (LOD) of the analytical system (≈ 0.1 fmol kg^{-1}/ ≈ 0.4 ppt at salinity 35 and potential temperature 4 °C). Furthermore, the use of SF_6 for deliberate

OSD
11, 2289–2335, 2014

tracer release experiments in the past might produce undefined offsets in concentrations in such areas and their surroundings (Tanhua et al., 2008).

2.2 Dichlorodifluoromethane

Dichlorodifluoromethane (CFC-12) was originally produced for applications as gas propellant and refrigerant. It is known as an ozone depleting compound with an atmospheric lifetime between 90–130 years (Minschwaner et al., 2013). The production was started in the late 1920s and phased out in the early 1990s due to its enormous environmental impact. Hence, the observational record of the atmospheric concentration shows a decreasing trend since the mid-1990s (Bullister, 2011). The sources of CFC-12 are only of anthropogenic origin with no significant sinks within the ocean. However, there are possible sinks in aqueous anoxic media (Hornemann et al., 2007) but this does not apply for anoxic regions in the ocean (Tanhua et al., 2005; Krysell et al., 1994; Lee et al., 2002, 1999). To this end, CFC-12 is an inert compound and usable as a transient tracer in the ocean. The concentration is stated in ppt, similar to SF_6. An upcoming problem is the decreasing concentration in the atmosphere. Values above the current atmospheric concentration describe two dates in the atmospheric history of CFC-12 which leads to undefined results within age analyses such as the tracer age and the TTD based mean age. This atmospheric concentration limit (ACL) denotes the upper limit of use of CFC-12, e.g. 528 ppt in the Northern Hemisphere and 526 ppt in the Southern Hemisphere in 2014. The lower limit of use is set by the LOD of $\approx 0.01\,\mathrm{pmol\,kg^{-1}} / \approx 7.7\,\mathrm{ppt}$ at salinity 35 and potential temperature 4 °C. Additionally, it is recommended to use the saturation correction due to the high emission rate of CFC-12 in the past which caused a temporarily undersaturation of surface waters (Tanhua et al., 2008).

OSD
11, 2289–2335, 2014

2.3 Tritium

Tritium (^{3}H or T) is a radioactive isotope of hydrogen with a half-life of 12.32 yr. It has a natural background concentration due to radiative induced formation processes in the stratosphere and gets usually oxidized to tritiated water (HTO). The extremely low concentration is commonly stated in Tritium Units (TU) where 1 TU is equivalent to 1 tritium atom per 10^{18} hydrogen atoms. The natural mean concentration in water vapor in air is 5.14 TU (1.66×10^{-2} pCi mL^{-1}) and 0.49 TU (1.6×10^{-3} pCi mL^{-1}) in the ocean surface (Cossairt, 2012). The anthropogenic sources are nuclear facilities and the nuclear bomb tests during the 1940s, 1950s and mainly the 1960s where large amounts of tritium were released into the atmosphere with an estimated total activity of 2.4×10^2 Bq (CNSC, 2009). The tritium input into the ocean depends on precipitation, river input and water vapor pressure at the air–sea interface. Mean tritium input functions (TIF), e.g. the TIF of the Atlantic Ocean by Dreisigacker and Roether (1978); Roether et al. (1992), automatically imply uncertainties based on local differences of the net input. Thus it is difficult to estimate a generally valid TIF without neglecting prominent regional impact factors. For example, distinct local influences on the surface tritium concentration can be found in the Mediterranean Sea which is characterized by a high net evaporation, large river runoff, dilution by Atlantic water and an intricate ventilation pattern (Stöven and Tanhua, 2014; Roether et al., 2013). Due to the possible uncertainties of a TIF it is recommended to use the isotope ratio of tritium and the decay product helium-3 (^{3}He$_{\text{trit}}$) for TTD applications. The isotopic ratio is given in percent of the tritium decay and stated as δ^3H in the following (Eqs. 1 and 2).

$$R = \frac{^3\mathrm{H}}{^3\mathrm{He}_{\mathrm{trit}}} = \left(e^{\lambda t} - 1\right)^{-1} \tag{1}$$

$$\delta^3\mathrm{H} = \frac{R}{1+R} \times 100 \tag{2}$$

Discussion Paper | Discussion Paper | Discussion Paper | Discussion Paper |

OSD

11, 2289–2335, 2014

Tracers in the Southern Ocean

T. Stöven et al.

This method requires additional measurements of helium and neon to separate the tritiugenic share of the total ^3He concentration (Eq. 3). In this equation $^3He_{tot}$ denotes the measured ^3He concentration in seawater, $^3He_{ex}$ the excess ^3He, which can be determined with neon data and $^3He_{ter}$ as the terrigenic part, released by the earth crust and mantle. The separation method is described by Roether et al. (2013). The terrigenic share has most influence on the uncertainty because it cannot be directly determined. Possible estimates are graphical methods (Aeschbach-Hertig, 1994) and kinematic models (Roether, 1989) which have been developed for the helium-tritium-dating method (Jenkins, 1977).

$$^3He_{trit} = {}^3He_{tot} - {}^3He_{ex} - {}^3He_{ter} \tag{3}$$

2.4 Argon-39

Argon-39 (^{39}Ar) is a noble gas isotope with a half-life of 269 yr. Similar to tritium it is mostly formed by cosmic ray interactions in the stratosphere with ^{40}Ar as main precursor. As a noble gas it is highly inert and there are no known sources or sinks in the ocean besides the radioactive decay. Thus, ^{39}Ar matches all requirements of a transient tracer. However, the measurement of ^{39}Ar is expensive, time-consuming and laborious. In contrast to CFCs, SF_6 and tritium it is not possible to use the common way of water sampling with Niskin bottles. One of the first measurement systems for environmental samples was based on low level decay counting (LLC) of 0.3–1 L of pure argon gas extracted from 1–3 tons of water per sample (Loosli, 1983; Schlitzer and Roether, 1985; Rodriguez, 1993). The concentration of ^{39}Ar is expressed as the isotopic ratio in water in relation to the isotopic ratio in the atmosphere (% modern). Despite of the obviously big stumbling blocks during sampling, and the enormous efforts that had to be put in the measurement facilities, the strong interest in this isotope and its scientific use have never ceded. Recently, a new method was developed to measure ^{39}Ar among other isotopes. The new technique is based on a laser induced atom counting method, the so called Atom Trap Trace Analysis (ATTA) (Jiang et al., 2011; Lu et al., 2014). This

OSD
11, 2289–2335, 2014
Tracers in the Southern Ocean
T. Stöven et al.

method allows for ^{39}Ar measurements from only 2.5 L of water down to an isotopic abundance of 8×10^{-16} (Jiang et al., 2011) which provides an efficient possibility of measuring ^{39}Ar as part of transient tracer surveys in the ocean in the near future, thus significantly enhancing the modest global dataset.

2.5 Carbon-14

Carbon-14 (^{14}C), also known as radiocarbon, is a radioactive isotope with a half-life of ≈ 5730 yr (Engelkemeir et al., 1949). As mentioned previously, the natural share of radioactive isotopes and thus radiocarbon is produced in the stratosphere, with CO_2 as the major component. Due to the biological interactions of CO_2 such as photosynthesis and respiration, radiocarbon can be detected in many natural organic and inorganic compounds. Once the interaction with the atmosphere is stopped (e.g. the death of an organism), radiocarbon serves as natural timer. W. F. Libby and co-workers developed the measurement technique and the dating method of radiocarbon in the first half of the 20th century (Libby, 1955). However, radiocarbon shows a significant alternating background concentration based on variability in the sun activity (DeVries-Effect) and the earth's geomagnetic field (Stuiver, 1961). The deviations in atmospheric concentrations are an essential part of the calibration routine when using the radiocarbon dating method. Furthermore, there are three additional natural and anthropogenic error sources which need to be considered. Since the industrialization started, the massive burning of fossil fuels with low radiocarbon content has led to a dilution of the natural atmospheric concentration, i.e. the Suess-Effect (Tans et al., 1979). This dilution was surpassed by atmospheric radiocarbon input during nuclear bomb-tests in the 1960s and also in minor share by nuclear power plants. Both effects, the dilution and the input of atmospheric radiocarbon, have their major origin in the Northern Hemisphere so that a gradient in ^{14}C occurs to the Southern Hemisphere. The third error source is the equilibration time of almost 10 years which leads to a permanent disequilibrium at the air–sea-boundary (Broecker and Peng, 1974). Information required for the application

OSD
11, 2289–2335, 2014

Title Page
Abstract Introduction
Conclusions References
Tables Figures
◀I ▶I
◀ ▶
Back Close
Full Screen / Esc
Printer-friendly Version
Interactive Discussion

with the TTD method is a known boundary condition at $C_0(t_s - t)$, i.e. the condition at the origin of the water parcel. Thus, the complex gas exchange and the spatial differences in atmospheric offsets complicate the use of radiocarbon as transient tracer in the ocean. Despite these problems, radiocarbon is a powerful tracer for water masses in the ocean, in particular those that are expected to be very old, e.g. in the deep basins of the northern Pacific.

Radiocarbon concentrations of oceanic measurements are commonly stated as $\Delta^{14}C$ in ‰ (Eqs. 4 and 5). The zero value of $\Delta^{14}C$ is defined by the used standard (usually A.D. 1950). Measurements are carried out with the accelerator mass spectrometry (AMS) technique. The LOD of this technique is an isotopic abundance of 10^{-15} (Libby, 1955) (Table 1) with a precision of 2–4.5‰. The sampling procedure is similar to the one of DIC samples with a volume of 0.5 L and poisoning to inhibit biological activity during storage.

$$\Delta^{14}C = \delta^{14}C - 2\left(\delta^{13}C + 25\right)\left(1 + \frac{\delta^{14}C}{1000}\right) \tag{4}$$

$$\delta^{14}C = \left[\frac{\left({}^{14}C/C\right)_{\text{sample}} - \left({}^{14}C/C\right)_{\text{std}}}{\left({}^{14}C/C\right)_{\text{std}}}\right]1000 \tag{5}$$

2.6 Limit of detection and quantification

The limit of detection (LOD) is usually defined as three times the standard deviation of the calibration blank (3σ) (CLSI, 2004). The sample size, e.g. the volume, can be adjusted (scaled up) to a certain extent to reach the needed concentration levels (see ^{39}Ar). Hereby, the robustness of the analytical method becomes the main factor due to an increasing sensitivity to contamination. Most of the transient tracer measurements are carried out with a variety of custom-made analytical systems, sampling methods and sample volumes. Together with further differences in sampling areas and other features (see Sect. 4.1) there are a number of specific LODs. To this end, the LODs stated in Table 1 are representing common mean LODs. The limit of quantification (LOQ) is differently described in analytical publications. In medical analysis the LOQ is defined as 10σ (CLSI, 2004) which would lead to several problems in ocean analytics especially in trace level analytics where the obtained values are often near the LOD. However, using values near the LOD automatically imply high uncertainties in data processing which are related to the precision and accuracy of the used analytical system (Stöven and Tanhua, 2014).

3 Transit time distribution

3.1 Ventilation concept

Mixing processes in the ocean are difficult to quantify due to the versatile combinations of underlying influencing factors. Considering only the major components, like advective and isopycnal diffusive processes, a practical model can be implemented, namely the Transit Time Distribution (Hall and Plumb, 1994). This model is based on the Green's function and the assumption of a steady and one-dimensional advective velocity and diffusion gradient. One possible solution of a TTD is the simplified analytical expression (Eq. 6), known as Inverse Gaussian transit time distribution (IG-TTD), where Γ is the mean age, Δ the width of the distribution and t the time range (Waugh et al., 2003). Equation (7) provides the link between the age spectrum $G(t)$ and concentration of a transient tracer $c(t_s, r)$ at year t_s and location r. The source concentration $c_0(t_s - t)$ is the concentration at source year $t_s - t$ related to the input function of a tracer.

OSD
11, 2289–2335, 2014

The exponential term accounts for the decay rate of radioactive transient tracers.

$$G(t) = \sqrt{\frac{\Gamma^3}{4\pi\Delta^2 t^3}} \cdot \exp\left(\frac{-\Gamma(t-\Gamma)^2}{4\Delta^2 t}\right) \tag{6}$$

$$c(t_s, r) = \int_0^\infty c_0(t_s - t) e^{-\lambda t} \cdot G(t, r) \mathrm{d}t \tag{7}$$

The Δ / Γ ratio of the TTD corresponds to the advective and diffusive characteristics of the fluid. Low Δ / Γ ratios between 0.2–0.8 describe a more advective water parcel whereas higher ratios between 1.2–1.8 describe a more dominant diffusive share of the mixing process. A Δ / Γ ratio higher than 1.8 leads to large uncertainties in mean age and should be avoided (Stöven and Tanhua, 2014). A Δ / Γ ratio of 1.0 is considered as the standard ratio which is applicable to many tracer surveys (Schneider et al., 2014, 2010; Tanhua et al., 2008; Waugh et al., 2006, 2004; Huhn et al., 2013). However, for more complex mixing structures, several approaches have been used to constrain the Δ / Γ ratio and thus the TTD based mean age (Stöven and Tanhua, 2014; Schneider et al., 2012; Waugh et al., 2002).

3.2 Input functions

The input functions are the essential part when using field data within a TTD model. Chronological transient tracers (CFCs, SF_6) depend on an increasing emission rate into the atmosphere, thus providing information about time. Data of atmospheric trace gas measurements at several locations in the world are provided by, for example, the AGAGE network with monthly updated data (Bullister, 2011). The distributed measurement points are necessary, because most of the anthropogenic trace gases are released by the industrial nations in the Northern Hemisphere. The atmospheric mixing is fast, however a small but significant concentration gradient between the Northern and Southern Hemisphere remains, which has to be accounted for. The equilibration time

OSD
11, 2289–2335, 2014

of the tracer, fast replenishment of surface waters, ice covered areas and wind speed are the main factors that influence the saturation state and can result in an under- or supersaturated water parcel. Possible states of undersaturation of CFC-12 and SF_6 at the air–sea boundary were found to be in the order of 10–60 % (Haine and Richards, 1995; DeGrandpre et al., 2006; Tanhua et al., 2008). Most of the natural radioactive transient tracers, such as ^{39}Ar, are independent of an input function due to a constant concentration level in the atmosphere. The formation processes of nuclides are usually radiatively initiated in the stratosphere and counterbalanced by the radioactive decay of the isotopes. Thus, natural isotopes are homogeneously distributed with only small variances in surface saturation in large parts of the ocean. However, the isotope effect needs to be additionally considered in terms of saturation besides the other aspects stated above. An isotope meets the demand of an ideal tracer for the TTD method, when there are no sources in the ocean and when a sufficient decay rate exists, serving as the only sink. Isotopes which are or were produced and released by nuclear power plants or nuclear bomb tests might have a significant local or global input function into the ocean which leads to several problems and restrictions in their use (see Sect. 2).

3.3 Mean age matrices

The TTD based concentration matrices are necessary to determine the mean age of a water sample (see Eq. 7). For chronological transient tracers, such as CFC-12 and SF_6, the atmospheric history, the year of sampling and the hemisphere are the required information for the calculations. In contrast, radioactive transient tracer concentrations depend only on the decay rate (^{39}Ar) and some additional factors (^{3}H, ^{14}C, see above). Figure 1 shows plots of the specific tracer concentration vs. mean age for different Δ / Γ-ratios, i.e. data plotted from TTD matrices. CFC-12 and ^{3}H both have a declining trend of the atmospheric concentration which leads to a sort of twist (anomaly) for high concentrations in the TTD matrix (Fig. 1c and d). The mean age becomes ambiguous because of a partly decreasing mean age with increasing Δ / Γ-ratio. But in contrast

OSD
11, 2289–2335, 2014

to the atmospheric concentration limit of CFC-12, such a distribution anomaly has no limiting influence within a TTD model.

Related to possible age information, each tracer has a specific time range. Figure 1a–f shows that SF_6 and ^3H are mainly applicable in younger to moderately old water masses, i.e. halocline and strongly ventilated water layers. CFC-12 is restricted in shallower layers due to the atmospheric concentration limit but provides time information for intermediate and deep water layers with significant ventilation due to deep water formation. ^{39}Ar extends the time range of CFC-12 due to the half-life of 269 years and the resulting slow decline of its concentration (Fig. 1e). It is a very useful transient tracer for old water masses (i.e. in less ventilated deep ocean basins). Similar to SF_6 and δ^3H it has also no restrictions besides the LOD which highlights another advantageous feature of ^{39}Ar. The use of ^{14}C stands and falls with the knowledge of the boundary conditions. A general TTD matrix can be calculated by using a boundary condition of $\Delta^{14}C = 0$ so that the measured concentrations (related to a standard) just need to be converted to this scale. ^{14}C is a tracer for very old water masses ($\Gamma > 300$) and thus can be used in the time range of ^{39}Ar and beyond.

3.4 Tracer couples and validity area

The TTD method can be constrained under certain assumptions using two transient tracers with sufficiently different input functions (Stöven and Tanhua, 2014). However, each combination of such a tracer couple has a specific validity area, i.e. time range of application which requires a common transient tracer unit. The different concentration units of the transient tracers can all be directly related to a tracer age (also known as apparent age) which provides a common tracer scale. The tracer age (τ) describes an age based on a purely advective flow in the ocean, neglecting any mixing processes. Equations (8) and (9) describe the tracer age for chronological transient tracers with $c(t_s)$ as concentration at sampling year t_s and the referred atmospheric concentration $c(t_{hist})$ at year t_{hist}. The tracer age of radioactive transient tracers can be determined by the decay function (Eq. 10) with c_i as the initial concentration, c the measured

OSD
11, 2289–2335, 2014

concentration and the decay rate λ. The tracer age of δ^3H basically depends on a similar decay function like Eq. (10) except that the equation is rewritten by using the decay product $^3He_{trit}$ instead of initial concentration (Eq. 11).

$$c(t_s) = c_0(t_{hist}) \tag{8}$$

$$\tau = t_s - t_{hist} \tag{9}$$

$$\tau = \frac{1}{\lambda} \cdot \ln\left(\frac{c_i}{c}\right) \tag{10}$$

$$\tau = \frac{1}{\lambda} \cdot \ln\left(1 + \frac{\left[^3He_{trit}\right]}{\left[^3H\right]}\right) \tag{11}$$

The first step to determine the validity area of a tracer couple is to convert the tracer concentrations of the TTD matrices into the corresponding tracer age. Then the TTD matrix of the tracer with the shorter time range is subtracted from the one with the longer time range, e.g. $\tau_{CFC\text{-}12}$–τ_{SF6}. The resulting matrix shows the required tracer age differences (TAD) of the tracer couple which belong to a specific combination of mean age and Δ/Γ-ratio. Figure 2a–g shows the different TADs and the resulting validity areas of the transient tracer combinations. The lower limiting case is always a TAD of 0 due to the fact that a pure advective flow at $\Delta/\Gamma = 0$ directly corresponds to the tracer age. The thick black lines with the adjacent white areas in Fig. 2 illustrate the individual restrictions of a tracer couple where the highest LOD denotes the most limiting case (see Table 1 for LODs). The LOD of δ^3H cannot directly be determined due to the uncertain amount of the initial input of tritium. In other words, the isotopic ratio is independent of the concentration levels at the source region and can either be in the analytical range of the measurement techniques or below the detection limit. Thus, tracer couples including δ^3H, i.e. ^{39}Ar / δ^3H (Fig. 2f), do not show limiting cases because they need to be determined for every tracer survey itself. The combination of ^{39}Ar and ^{14}C shows also no restrictions in the range of the oceanic mean age shown

OSD
11, 2289–2335, 2014

(Fig. 2g). The concentration contour lines are highlighted in black and white of either tracer one or tracer two of the couple (see figure caption for more information).

The concept of validity areas by TAD provide reliable results of constrainable or non-constrainable tracer data sets within the IG-TTD model. Therefore, the TADs of the measured transient tracers at the particular sampling points are determined and then compared with the belonging TAD matrix. For tracer data with higher TAD values than presented in Fig. 2 the IG-TTD model cannot provide significant and reasonable results so that other models are necessary to describe the ventilation in such ocean areas.

4 Southern Ocean ventilation

4.1 Transient tracer data

In the following we use SF_6, CFC-12 and ^{39}Ar data which represent transient tracers with a short and long time range, i.e. transient tracers which can be applied to well and less well ventilated water masses. This includes a new data set of CFC-12 and SF_6 which was obtained during the ANT-XXVIII/3 expedition from 7 January to 11 March 2012 from Cape Town, South Africa to Punta Arenas, Chile on the German research vessel *Polarstern* (Wolf-Gladrow, 2013). Figure 3 shows the three sampling regions of CFC-12 and SF_6 with 691 samples each at 57 stations. The sampling procedure and measurement system (VS1) is identical as described in (Stöven and Tanhua, 2014). The data was corrected with 0.15 (±0.02) fmol kg^{-1} for SF_6 and 0.01 (±0.003) pmol kg^{-1} for CFC-12 due to a permanent offset of the ampule blank which was contributed to a non-reparable leak of a magnetic valve between the vacuum purge tower and the sample ampule. The blank offset was continuously rechecked as part of the robust quality control routine described in Stöven (2011). Furthermore, the LOD was depending on the wave height which had direct impact on the baseline noise of the gas chromatograph. With increasing wave height, the baseline started to oscillate and became more noisy. This was probably caused by a marginal unsteadiness

OSD
11, 2289–2335, 2014

in the gas supply (pressure deviation at the gas in or out). The maximum elevated LOD value of 0.36 fmol kg^{-1} for SF_6 was observed during a storm with wind force 10–11 bft and a mean wave height of 8–9 m. Surface measurements a few hours after the storm showed significant supersaturation of SF_6 in the range of 20–50 % (Fig. 4). The surface saturation of CFC-12 shows only minor elevations which is probably contributed to the bubble effect having much more impact on less soluble gases like SF_6.

The precision of ±3.6 %/0.03 fmol kg^{-1} for SF_6 and ±0.8 %/0.015 pmol kg^{-1} for CFC-12 is significantly lower than those of the measurements at cruise M84/3 in 2011. This can be attributed to some specific conditions during the new cruise, which are documented in the following. The detailed documentation of the sampling protocol includes a list of all leaks and conspicuous features regarding Niskin bottles. There have been several CTD-casts where valves were not sufficiently tightened, gaskets or one of the plugs leaky. Comparing the sampling lists with the data set and especially with the outliers clearly shows that there have been some sort of carry-over of water fractions in many of the Niskin bottles. Finally, if there could be observed apparent leaks of the Niskin, the data was stated as probably bad within the quality control process which leads to several complete stations being discarded. A general quality control of the Niskin bottles should be part of the operating process which also requires the availability of spare parts, such as O-Rings and other gasket parts. The data will be available at the Carbon Dioxide Information Analysis Center (CDIAC) data base later this year. The second data set containing CFC-12 and SF_6 data was collected during the SWEDARP expedition in January–February 1998 on board the research vessel *S.A. Agulhas* (Turner et al., 2004). The section from 60.30° S to 41.30° S along 6° E is very close to the section along 10° E of the ANT-XXVIII/3 expedition. The section includes 38 stations with a maximum depth of 3100 m due to the limited wire length on the winch. Two GC-ECD system were used for on board measurements where the SF_6 measurement system is similar to Law et al. (1994) and the CFC-12 measurement system to Grasshoff et al. (1999). The data, sampling and measurement procedure is

OSD
11, 2289–2335, 2014

discussed by Tanhua et al. (2004). The precision is ±3.1 %/0.06 fmol kg^{-1} for SF_6 and ±0.7 %/0.03 pmol kg^{-1} for CFC-12.

Ocean data of ^{39}Ar is still rare due to the enormous efforts which had to be made for a single measurement. To this end, available data was taken from Rodriguez (1993) which represents measurements of water masses north and south of the 1998 and 2012 sections (Table 2). The northern data consists of samples of deep water layers in the eastern Atlantic and the southern data of measurements in the whole water column near the south-east end of the Weddell Sea. The sampling for one measurement was based on four 250 L Gerard Ewing samplers distributed over a depth range of 400 m so that every data point describes the corresponding mean value. The measurements were conducted at the University of Bern using the LLC method with a given relative error of 10–14 % (Schlitzer and Roether, 1985). The sampling and measurement procedure as well as data statistics are discussed by Loosli (1983) and Rodriguez (1993).

4.2 Ventilation analysis

Figure 5a shows the CFC-12 concentration along 10° E from 44.0–53.0° S of the ANT-XXVIII/3 cruise in 2012. Minimum CFC-12 concentrations down to 25 ppt were observed in the northern part between 44–46° S (stations 57–63) in a depth range of 2000–3500 m. This layer represents the southwards spreading North Atlantic Deep Water (NADW) (Whitworth and Nowlin, 1987; Pardo et al., 2012), which in Fig. 6 is discernible as a salinity maximum at a potential temperature of ≈ 2–3 °C. This low CFC-12 concentration layer extends further southwards across the Subantarctic Front (SAF) at 46° S and it steadily shoals with an increasing concentration up to ≈ 45 ppt at the Polar Front (PF) at 51° S. The elevation of the NADW core and the increasing concentration is caused by mixing with underlying Lower Circumpolar Deep Water (LCDW) and overlying Upper Circumpolar Deep Water (UCDW) which represent the main volume share within the Antarctic Circumpolar Current (ACC) in the frontal system. LCDW is less salty but colder than NADW and can be identified throughout the whole section

OSD
11, 2289–2335, 2014
Tracers in the Southern Ocean
T. Stöven et al.

with near bottom concentrations of CFC-12 between 40–50 ppt (Figs. 5a and 6). The transition between the water layers of UCDW and the NADW core is less clear but delimited by the salinity minimum of the relatively warm ($\Theta = 3\,^{\circ}$C) Antarctic Intermediate Water (AAIW) and CFC-12 concentrations higher than 200 ppt. The elevated and relative homogeneous concentrations of 50–60 ppt in the southern part between 51–53° S (stations 78–84) from 1500 m-bottom are related to Circumpolar Deep Water with water mass properties deriving from NADW and Antartic Bottom Water (AABW). The AABW is formed in the shelf regions of Antarctica. In this case it probably carries the properties of Weddell Sea Deep Water (WSDW) which indicates the Weddell Sea coastal regions as source region. AABW propagates northwards along the bottom contour in a clockwise direction from its source region and forms a more dense bottom layer than LCDW and the southward propagating NADW (Whitworth and Nowlin, 1987; Orsi et al., 1999; Stramma and England, 1999). AABW characteristics can be found between 51–53° S with CFC-12 bottom concentration of 50–70 ppt (Figs. 5a and 6).

The ACC is driven and enforced by strong westerly winds, inducing a significant Ekman transport with northwards flowing surface waters. Divergence and convergence of the Ekman transport leads to local upwelling and downwelling of density surfaces, forming overturning circulation called the Deacon Cell. As an indicator of the Deacon Cell, the very strong vertical concentration gradient between the surface waters (> 500 ppt) and the underlying deeper waters (< 100 ppt) clearly shoals towards the south, from 1250 m to shallower than 500 m along the 2012 section. An additional factor that influences the Deacon Cell circulation is the increasing stability of the halocline due to cold surface and intermediate waters, inhibiting convection to intermediate depths in this region. Note that the shoaling of the transition layer is also shown along 6° E from 43.5–60.4° S of the SWEDARP cruise in 1998 (Fig. 5b). Compared with the data set of 2012, similar tracer structures were found. The tracer concentrations are < 20 ppt below 1750 m in the northern part (stations 382–385), pointing to NADW, and elevated concentrations of > 45 ppt between 48–58° S (stations 266–281) in the deep water indicating CDW and Weddell Sea Deep Water (WSDW). The enhanced distances between

OSD
11, 2289–2335, 2014

Tracers in the Southern Ocean

T. Stöven et al.

the stations 382–288 and 266–262 as well as the limited sampling depth prohibit a further section analysis.

The SF_6 data of 1998 and 2012 show similar features to the CFC-12 data, e.g. the Deacon Cell effect (Fig. 5c and d). Due to the relatively young atmospheric history of SF_6, the tracer is limited to the upper 1000 m in 1998. However, in 2012, the detection limit was between 1200–1500 m north of 51° S. Although the atmospheric concentration of SF_6 doubled in the 14 years between the cruises, the only change in the ocean is an increase of the vertical gradient, and no significant intrusions into deeper layers. The tracer input is based on subduction of surface waters to intermediate depths, e.g. a relatively advective AAIW, with a sharp boundary to the underlying water. Further southwards of 51° S, SF_6 was detectable down to the bottom with concentrations of $\approx 0.3\,\mathrm{fmol\,kg^{-1}}$ (Fig. 5c). Some weak signals near the LOD could be observed in the bottom layer between 47–51° S indicating SF_6 in the outer branches of AABW. The core of NADW contains SF_6 below the LOD or is absent.

The sections of 1998 and 2012 are separated into a northern and southern part (blue and red bars in Fig. 5a–d) for further analyses which allows for a comparison between water mass properties in the northern and southern part of the ACC system and the temporal variations between the 14 years of both tracer surveys. The CFC-12 and SF_6 profiles of the chosen northern and southern investigation areas were recalculated to single mean profiles for both years (Fig. 7a and b). The standard deviation of the mean profiles can be found in the appendix (Tables A1–A4). Figure 7a and b clearly shows the large differences in the halocline structure of both tracers with a smooth transition in the north which turns into a very sharp one in the south. The mean profile of SF_6 in the southern part shows a significant minimum at 1500 m depth (dashed black line in Fig. 7b) which is contributed to the influence of SF_6 free water masses. The transition between tracer free and low level tracer concentrations, e.g. $< 0.1\,\mathrm{fmol\,kg^{-1}}$ of SF_6, leads to high uncertainties. Hence, ventilation processes near such a transition cannot be analyzed with the concerning tracer due to the insignificant or missing time information.

OSD
11, 2289–2335, 2014

The tracer age difference (TAD) of CFC-12 and SF_6 is shown in Fig. 7. Note that not only the TAD, but also the concentration of the tracers needs to be considered, when the TAD method is used. The TAD in the northern part in 1998 was −3 years in the surface, probably caused by saturation effects and between 2–5 years down to 1100 m depth where the detection limit of SF_6 was reached (solid blue line in Fig. 7). According to the validity area of the tracer couple in the Southern Hemisphere in 1998 (Fig. 8a) and 2012 (Fig. 8b) the IG-TTD can only be constrained for the northern part. Furthermore, the increase of the time range between the validity areas in 1998 and 2012 clearly show that SF_6 became a powerful transient tracer during the last 14 years.

The southern part has TADs between 6–12 years and thus the data is out of the application limit of the IG-TTD (dashed blue line in Fig. 7c). The data set of 2012 shows quite similar characteristics. The atmospheric concentration limit of CFC-12 occurs since 2001 and reached down to 300 m in 2012 in the northern part (red line in Fig. 7d), so that no results could be obtained for shallower water layers. In contrast to the steady TAD in 1998 in the northern part, the TAD in 2012 decreases with depth from 11 to 2 years (solid black line in Fig. 7c) and thus it is also in the range of a constrainable IG-TTD (Fig. 8a). The TAD in the southern part (dashed black line in Fig. 7c) has a maximum of 18 years at 100 m, a steady TAD of 10–13 years between 350–1000 m and 2000–4000 m. Similar to the northern TAD in 2012 and the southern TAD in 1998, the southern TAD in 2012 shows a fast declining trend below 1000 m which is the transition area to SF_6 free water masses and thus reliable conclusions cannot be drawn. Both sections clearly show a rapid change in the ventilation pattern between 47.0–50.0° S which can be related to the transition between the SAF and PF. The northern part south to 46° S can be reasonably described with the IG-TTD model which agrees with the results of several investigations (Waugh et al., 2006; Schneider et al., 2012). In contrast, the IG-TTD cannot be used in the Southern Ocean south of about 46–47° S.

Table 3 shows the constrained Δ / Γ ratios and the mean age of the northern part in 1998 and 2012. The error is based on the precision and accuracy of the measurement techniques and possible deviations of the purge efficiency and saturation of the tracer

OSD
11, 2289–2335, 2014

(Stöven and Tanhua, 2014). The error range in 1998 is greater than in 2012 which can be related to the short atmospheric history of SF_6, i.e. lower concentration levels lead to larger error ranges. This shows again the positive development of SF_6 as a transient tracer. The Δ / Γ ratios from 1998 do not show a clear trend due to the relatively high uncertainty whereas the Δ / Γ ratios in 2012 are more or less the standard ratio of 1.0 down to 1000 m and thus consistent with several transient tracer investigations in the Atlantic Ocean (Schneider et al., 2012; Waugh et al., 2006, 2004). The water masses below 1000 m again describe the transition area of SF_6 where tracer free water parcels influence the distribution but not the calculated error range.

The mean age of both tracer surveys show only small changes (0–4 years) in the upper 600 m (Fig. 7d) and becomes indistinct below this depth. The water layers between 600–1000 m indicate that the water masses became slightly older with an increased mean age of up to 80 years in 2012. Due to the natural restriction, namely, the absence in earlier years of SF_6 it is not possible to analyze water masses below a depth of 1000 m. However, the 14 years between both tracer surveys allow for a time lag analysis which can identify changes in ventilation (Tanhua et al., 2013). This method is based on the similar atmospheric increase rates of CFC-12 and SF_6. It is simply the tracer age difference of historic CFC-12 and modern SF_6 data ($\Delta\tau = \tau(SF_6) - \tau(\text{CFC-12})$) with a 14 year time lag between both data sets, e.g. 1998–2012. A $\Delta\tau$ of 0 indicates no change in ventilation whereas positive values denote a decrease and negative values an increase of ventilation. Figure 9 describes the $\Delta\tau$ between the CFC-12 tracer age of 1998 and the tracer age of SF_6 in 2012 for the northern and southern part. The northern part shows an increase in ventilation in the upper 800 m and a decrease below this depth. The minor deviations of $\Delta\tau = \pm 2$ years between 300–1000 m are in good agreement with the findings of the TTD method considering the error range of the constrained mean age. The southern part shows a higher increase in ventilation between 0–1000 m than the northern part and a steady ventilation can be found below 2000 m. However, these findings are not in line with the recently published work by

OSD
11, 2289–2335, 2014

Waugh et al. (2013) who used an assimilated model and a TTD model with standard ratio to predict CFC-12 concentrations of repeated sections in the Southern Ocean.

Because of the absence of SF_6 below 1200 m it is not possible to constrain the IG-TTD in the deep water of the Southern Ocean. To this end, a theoretical approach is carried out by using ^{39}Ar data from the early 1980s (Fig. 10) which were recalculated to a possible concentration range in 2012. It was assumed that the ^{39}Ar in the Weddell Sea was supplied by either steady ventilation, i.e. the decay is counterbalanced by water renewal, or zero ventilation with ^{39}Ar decay only. The ^{39}Ar in the eastern Atlantic was assumed to be affected by an increased or decreased ventilation (±15 years in tracer age). The ^{39}Ar data from the eastern Atlantic was supposed to be correlated with the water mass properties of the northern part of the section in 2012 and ^{39}Ar in the Weddell Sea likewise to the southern part. Figure 11a and b show the theoretical TAD between CFC-12 and the estimated concentration range of ^{39}Ar (grey shaded area). The red line in both figures denotes the application limit of the IG-TTD model, defined by the maximum tracer age difference between CFC-12 and ^{39}Ar (see Fig. 2). Here again, it is highlighted that even with another tracer couple and with generously set concentration ranges of ^{39}Ar, it is not possible to constrain the IG-TTD in the southern part of the ACC whereas the northern part would be constrainable for the complete estimated range. For ocean areas where the IG-TTD is valid, a tracer couple consisting of ^{39}Ar and CFC-12 could provide significant information about ventilation in deep water layers which can not be achieved with SF_6 at present.

5 Conclusions

Transient tracers in combination with the IG-TTD are a powerful tool to investigate ocean ventilation. To analyze well ventilated water masses, SF_6 and δ^3H should be used due to the young atmospheric history and high decay rate, respectively. CFC-12 shows a declining trend in the atmosphere since 2001, which leads to ambiguous results in tracer age and mean age for values above this atmospheric concentration

OSD
11, 2289–2335, 2014

limit (ACL). This restriction only effects surface waters and to a certain extend also intermediate waters at present, so that CFC-12 data still plays a major role in the analysis of deep water ventilation. ^{39}Ar has a low decay rate, which provides a larger time range than CFC-12. Thus it is a useful tracer for less ventilated water masses, e.g. deep ocean basins in the Pacific Ocean. The recent developments of the ATTA method provide a more simple sampling and measurement of ^{39}Ar than in the past so that it will become more in focus in future work. The ambiguous or unknown boundary conditions of radiocarbon complicate the application of the IG-TTD model so that other transient tracers are recommended to use.

The IG-TTD can be empirically constrained by using a transient tracer couple. Each tracer couple has a specific validity area, e.g. CFC-12 and SF_6 for intermediate and CFC-12 and ^{39}Ar for deep water masses. The concept of a tracer age difference (TAD) provides information about the validity area of a tracer couple and also the application limits of the IG-TTD. Data sets of transient tracer surveys in the ocean can be simply checked, if the IG-TTD can be applied or not. The radioactive transient tracers have constant validity areas in time which is based on their steady boundary conditions. However, the chronological transient tracers depend on their atmospheric history and thus a changing boundary condition which has directly impact on the validity area. For example, the atmospheric concentration of SF_6 almost doubled between 1998 and 2012, which led to an increase of the maximum mean age from 200 up to 500 years.

The Antarctic Circumpolar Current (ACC) in the Southern Ocean is a phenomenon with significant effects on water mass ventilation in the entire water column. Sections across the ACC of CFC-12 and SF_6 in 1998 (along 6° N) and in 2012 (along 10° N), both show the transition between the application area and limit of the IG-TTD. The Subantarctic Front (SAF) at 46° S denotes the application limit of the IG-TTD. The constrained IG-TTD north of the SAF provides mean age results only for the upper 1200 m due to the absence of SF_6 below this depth. The Δ / Γ ratio is near the standard ratio of 1.0 in 2012 with an increasing mean age of 0–80 years with increasing depth. The Δ / Γ ratios and mean age are slightly lower in 1998 whereas the time lag analysis

OSD
11, 2289–2335, 2014

indicate a small increase in ventilation in the upper 800 m and a decrease below. This difference can be contributed to the higher uncertainty of SF_6 in 1998. Furthermore the time lag analysis shows also an even higher increase in ventilation south of the SAF in the upper 1000 m and a steady ventilation between 2000 m-bottom.

The IG-TTD can be applied to large parts in the ocean but reaches its limits where complex ventilation pattern prevail. The Southern Ocean ventilation involves diapycnal mixing in some regions and depth ranges (Naveira Garabato et al., 2004) and other models are required to analyze such ventilation processes.

Acknowledgements. This work was supported by the Deutsche Forschungsgemeinschaft (DFG) in the framework of the priority programme "Antarctic Research with comparative investigations in Arctic ice areas" by a grant to T. Tanhua and M. Hoppema: Carbon and transient tracers dynamics: a bi-polar view on Southern Ocean eddies and the changing Arctic Ocean (TA 317/5, HO 4680/1). Partial support to T. Tanhua and M. Hoppema was received from EU FP7 project CARBOCHANGE "Changes in carbon uptake and emissions by oceans in a changing climate" (European Community's 7th Framework Programme, grant agreement no. 264879). We are grateful to the Alfred-Wegener-Institut for participation in *Polarstern* cruise "Eddy Pump". We like to thank V. Strass for his support during the expedition and the provision of the CTD bottle data. We are happy to acknowledge the great support by the master and crew of *Polarstern*, the chief scientist and the scientific party. Special thanks goes to Boie Bogner for his technical support during the ANT-XXVIII/3 cruise.

The service charges for this open access publication
have been covered by a Research Centre of the
Helmholtz Association.

References

Aeschbach-Hertig, W.: Helium und Tritium als Tracer für physikalische Prozesse in Seen, Ph.D. thesis, ETH Zürich, 1994. 2295

Bolin, B. and Rodhe, H.: A note on the concepts of age distribution and transit time in natural reservoirs, Tellus, 25, 58–62, doi:10.1111/j.2153-3490.1973.tb01594.x, 1973. 2291

Broecker, W. S. and Peng, T. H.: Gas exchange rates between air and sea, Tellus, 26, 21–35, doi:10.1111/j.2153-3490.1974.tb01948.x, 1974. 2296

Bullister, J. L.: Atmospheric CFC-11, CFC-12, CFC-113, CCl_4 and SF_6 Histories (1910–2011), Carbon Dioxide Information Analysis Center, available at: http://cdiac.ornl.gov/oceans/new_atmCFC.html (last access: 14 October 2014), 2011. 2293, 2299

CLSI: Protocols for Determination of Limits of Detection and Limits of Quantification, approved Guideline, CLSI document EP17, Clinical and Laboratory Standards Institute, Wayne, PA USA, 2004. 2297, 2298

CNSC: Investigation of the Environmental Fate of Tritium in the Atmosphere, INFO-0792, minister of Public Works and Government Services Canada, Canadian Nuclear Safety Commission, 2009. 2294

Cossairt, J. D.: Background levels of tritium, Environmental Protection Note, 28, 1–4, 2012. 2294

DeGrandpre, M. D., Koertzinger, A., Send, U., Wallace, D. W. R., and Bellerby, R. G. J.: Uptake and sequestration of atmospheric CO_2 in the Labrador Sea deep convection region, Geophys. Res. Lett., 33, L21S03, doi:10.1029/2006GL026881, 2006. 2300

Dreisigacker, E. and Roether, W.: Tritium and ^{90}Sr in North Atlantic surface water, Earth Planet. Sc. Lett., 38, 301–312, 1978. 2294

Engelkemeir, A. G., Hamill, W. H., Inghram, M. G., and Libby, W. F.: The half-life of radiocarbon (^{14}C), Phys. Rev., 75, 1825, doi:10.1103/PhysRev.75.1825, 1949. 2296

Grasshoff, K., Kremling, K., and Ehrhardt, M.: Methods of Seawater Analysis, Wiley-VCH, Weinheim, 1999. 2304

Haine, T. W. N. and Richards, K. J.: The influence of the seasonal mixed layer on oceanic uptake of CFCs, J. Geophys. Res.-Oceans, 100, 10727–10744, doi:10.1029/95JC00629, 1995. 2300

Hall, T. M. and Plumb, R. A.: Age as a diagnostic of stratospheric transport, J. Geophys. Res., 99, 1059–1070, 1994. 2291, 2298

Hornemann, A., Stute, M., Schlosser, P., Smethie, W., Santella, N., Ho, D. T., Mailloux, B., Gorman, E., Zheng, Y., and van Geen, A.: Degradation rates of CFC-11, CFC-12 and CFC-113 in anoxic shallow quifers of Araihazar, Bangladesh, J. Contam. Hydrol., 97, 27–41, 2007. 2293

OSD
11, 2289–2335, 2014

Tracers in the Southern Ocean

T. Stöven et al.

Huhn, O., Rhein, M., Hoppema, M., and van Heuven, S.: Decline of deep and bottom water ventilation and slowing down of anthropogenic carbon storage in the Weddell Sea, 1984–2011, Deep-Sea Res. Pt. I, 76, 66–84, doi:10.1016/j.dsr.2013.01.005, 2013. 2299

Jenkins, W. J.: Tritium-helium dating in the Sargasso Sea: a measurement of oxygen utilization rates, Science, 196, 291–292, doi:10.1126/science.196.4287.291, 1977. 2295

Jiang, W., Williams, W., Bailey, K., Davis, A. M., Hu, S. M., Lu, Z. T., O'Connor, T. P., Purtschert, R., Sturchio, N. C., Sun, Y. R., and Mueller, P.: ^{39}Ar detection at the 10^{-16} isotopic abundance level with atom trap trace analysis, Phys. Rev. Lett., 106, 103001, doi:10.1103/PhysRevLett.106.103001, 2011. 2295, 2296

Krysell, M., Fogelqvist, E., and Tanhua, T.: Apparent removal of the transient tracer carbon tetrachloride from anoxic seawater, Geophys. Res. Lett., 21, 2511–2514, doi:10.1029/94GL02336, 1994. 2293

Law, C. S., Watson, A. J., and Liddicoat, M. I.: Automated vacuum analysis of sulphur hexafluoride in seawater: derivation of the atmospheric trend (1970–1993) and potential as a transient tracer, Mar. Chem., 48, 57–69, 1994. 2304

Lee, B.-S., Bullister, J. L., and Whitney, F. A.: Chlorofluorocarbon CFC-11 and carbon tetrachloride removal in Saanich Inlet, an intermittently anoxic basin, Mar. Chem., 66, 171–185, doi:10.1016/S0304-4203(99)00039-0, 1999. 2293

Lee, B.-S., Bullister, J. L., Murray, J. W., and Sonnerup, R. E.: Anthropogenic chlorofluorocarbons in the Black Sea and the Sea of Marmara, Deep-Sea Res. Pt. I, 49, 895–913, doi:10.1016/S0967-0637(02)00005-5, 2002. 2293

Libby, W. F.: Radiocarbon Dating, Univ. of Chicago Press, Chicago, Ill., 1955. 2296, 2297

Loosli, H. H.: A dating method with ^{39}Ar, Earth Planet. Sc. Lett., 63, 51–62, 1983. 2295, 2305

Lu, Z.-T., Schlosser, P., Smethie Jr., W. M., Sturchio, N. C., Fischer, T. P., Kennedy, B. M., Purtschert, R., Severinghaus, J. P., Solomon, D. K., Tanhua, T., and Yokochi, R.: Tracer applications of noble gas radionuclides in the geosciences, Earth-Sci. Rev., 138, 196–214, doi:10.1016/j.earscirev.2013.09.002, 2014. 2295

Minschwaner, K., Hoffmann, L., Brown, A., Riese, M., Müller, R., and Bernath, P. F.: Stratospheric loss and atmospheric lifetimes of CFC-11 and CFC-12 derived from satellite observations, Atmos. Chem. Phys., 13, 4253–4263, doi:10.5194/acp-13-4253-2013, 2013. 2293

Naveira Garabato, A. C., Polzin, K. L., King, B. A., Heywood, K. J., and Visbeck, M.: Widespread intense turbulent mixing in the Southern Ocean, Science, 303, 210–213, 2004. 2312

Orr, J. C., Fabry, V. J., Aumont, O., Bopp, L., Doney, S. C., Feely, R. A., Gnanadesikan, A., Gruber, N., Ishida, A., Joos, F., Key, R. M., Lindsay, K., Maier-Reimer, E., Matear, R., Monfray, P., Mouchet, A., Najjar, R. G., Plattner, G. K., Rodgers, K. B., Sabine, C. L., Sarmiento, J. L., Schlitzer, R., Slater, R. D., Totterdell, I. J., Weirig, M. F., Yamanaka, Y., and Yool, A.: Anthropogenic ocean acidification over the twenty-first century and its impact on calcifying organisms, Nature, 437, 681–686, doi:10.1038/nature04095, 2005. 2291

Orsi, A. H., Johnson, G. C., and Bullister, J. L.: Circulation, mixing, and production of Antarctic Bottom Water, Prog. Oceanogr., 43, 55–109, 1999. 2306

Pardo, P. C., Perez, F. F., Velo, A., and Gilcoto, M.: Water masses distribution in the Southern Ocean: improvement of an extended OMP (eOMP) analysis, Prog. Oceanogr., 103, 92–105, doi:10.1016/j.pocean.2012.06.002, 2012. 2305

Ravishankara, A. R., Solomon, S., Turnipseed, A. A., and Warren, R. F.: Atmospheric lifetimes of long-lived halogenated species, Science, 259, 194–199, doi:10.1126/science.259.5092.194, 1993. 2292

Rodriguez, J.: Beiträge zur Verteilung von ^{39}Ar im Atlantik, Ph.D. thesis, University of Bern, Switzerland, 1993. 2295, 2305, 2319

Roether, W.: On oceanic boundary conditions for tritium, on tritiugenic ^{3}He, and on the tritium-^{3}He age concept, in: Oceanic Circulation Models: Combining Data and Dynamics, edited by: Anderson, D. and Willebrand, J., Vol. 284 of NATO ASI Series, Springer, the Netherlands, 377–407, doi:10.1007/978-94-009-1013-3_12, 1989. 2295

Roether, W., Schlosser, P., Kuntz, R., and Weiss, W.: Transient-tracer studies of the thermohaline circulation of the Mediterranean, Reports in Meteorology and Oceanography, 41, 291–317, 1992. 2294

Roether, W., Jean-Baptiste, P., Fourré, E., and Sültenfuß, J.: The transient distributions of nuclear weapon-generated tritium and its decay product ^{3}He in the Mediterranean Sea, 1952–2011, and their oceanographic potential, Ocean Sci., 9, 837–854, doi:10.5194/os-9-837-2013, 2013. 2294, 2295

Sabine, C. L. and Tanhua, T.: Estimation of anthropogenic co_2 inventories in the ocean, Annu. Rev. Mar. Sci., 2, 175–198, doi:10.1146/annurev-marine-120308-080947, 2010. 2291

Schlitzer, R. and Roether, W.: A meridional ^{14}C and ^{39}Ar section in Northeast Atlantic deep water, J. Geophys. Res., 90, 6945–6952, 1985. 2295, 2305

Schlosser, P., Bayer, R., Bönisch, G., Cooper, L. W., Ekwurzel, B., Jenkins, W. J., Khatiwala, S., Pfirman, S., and Smethie, W. M.: Pathways and mean residence times of dissolved pollutants in the ocean derived from transient tracers and stable isotopes, Sci. Total Environ., 237–238, 15–30, doi:10.1016/S0048-9697(99)00121-7, 1999. 2291

Schneider, A., Tanhua, T., Koertzinger, A., and Wallace, D. W. R.: High anthropogenic carbon content in the eastern Mediterranean, J. Geophys. Res., 115, C12050, doi:10.1029/2010JC006171, 2010. 2299

Schneider, A., Tanhua, T., Koertzinger, A., and Wallace, D. W. R.: An evaluation of tracer fields and anthropogenic carbon in the equatorial and the tropical North Atlantic, Deep-Sea Res. Pt. I, 67, 85–97, doi:10.1016/j.dsr.2012.05.007, 2012. 2299, 2308, 2309

Schneider, A., Tanhua, T., Roether, W., and Steinfeldt, R.: Changes in ventilation of the Mediterranean Sea during the past 25 year, Ocean Sci., 10, 1–16, doi:10.5194/os-10-1-2014, 2014. 2299

Stöven, T.: Ventilation processes of the Mediterranean Sea based on CFC-12 and SF_6 measurements, GEOMAR OceanRep, available at: http://oceanrep.geomar.de/id/eprint/13936 (last access: 14 October 2014), diploma thesis, Christian-Albrechts-Universität zu Kiel, 2011. 2303

Stöven, T. and Tanhua, T.: Ventilation of the Mediterranean Sea constrained by multiple transient tracer measurements, Ocean Sci., 10, 439–457, doi:10.5194/os-10-439-2014, 2014. 2291, 2292, 2294, 2298, 2299, 2301, 2303, 2309

Stramma, L. and England, M.: On the water masses and mean circulation of the South Atlantic Ocean, J. Geophys. Res., 104, 20863–20883, 1999. 2306

Stuiver, M.: Variations in radiocarbon concentration and sunspot activity, J. Geophys. Res., 66, 273–276, doi:10.1029/JZ066i001p00273, 1961. 2296

Tanhua, T., Olsson, K. A., and Fogelqvist, E.: A first study of SF_6 as a transient tracer in the Southern Ocean, Deep-Sea Res. Pt. II, 51, 2683–2699, doi:10.1016/j.dsr2.2001.02.001, 2004. 2305

Tanhua, T., Olsson, K. A., and Jeansson, E.: Formation of Denmark Strait overflow water and its hydro-chemical composition, J. Mar. Syst., 57, 264–288, doi:10.1016/j.jmarsys.2005.05.003, 2005. 2293

Tanhua, T., Waugh, D. W., and Wallace, D. W. R.: Use of SF_6 to estimate anthropogenic CO_2 in the upper ocean, J. Geophys. Res., 113, 2156–2202, doi:10.1029/2007JC004416, 2008. 2293, 2299, 2300

Discussion Paper | Discussion Paper | Discussion Paper | Discussion Paper |

Title Page
Abstract | Introduction
Conclusions | References
Tables | Figures
◀| |▶
◀ ▶
Back | Close
Full Screen / Esc
Printer-friendly Version
Interactive Discussion

Tanhua, T., Waugh, D. W., and Bullister, J. L.: Estimating changes in ocean ventilation from the early 1990s CFC-12 and late SF_6 measurements, Geophys. Res. Lett., 40, 927–932, doi:10.1002/grl.50251, 2013. 2309

Tans, P. P., de Jong, A. F. M., and Mook, W. G.: Natural atmospheric ^{14}C variations and the Suess effect, Nature, 280, 826–828, doi:10.1038/280826a0, 1979. 2296

Turner, D. R., Bertilsson, S., Fransson, A., and Pakhomov, E.: The SWEDARP 1997/98 marine expedition: overview, Deep-Sea Res. Pt. II, 51, 2543–2556, doi:10.1016/j.dsr2.2003.08.006, 2004. 2304

Waugh, D. W., Vollmer, M. K., Weiss, R. F., Haine, T. W. N., and Hall, T. M.: Transit time distributions in Lake Issyk-Kul, Geophys. Res. Lett., 29, 841–844, doi:10.1029/2002GL016201, 2002. 2299

Waugh, D. W., Hall, T. M., and Haine, T. W. N.: Relationships among tracer ages, J. Geophys. Res., 108, 3138, doi:10.1029/2002JC001325, 2003. 2291, 2298

Waugh, D. W., Haine, T. W. N., and Hall, T. M.: Transport times and anthropogenic carbon in the subpolar North Atlantic Ocean, Deep-Sea Res. Pt. I, 51, 1475–1491, 2004. 2299, 2309

Waugh, D. W., Hall, T. M., McNeil, B. I., Key, R., and Matear, R. J.: Anthropogenic CO_2 in the oceans estimated using transit time distributions, Tellus B, 58, 376–389, 2006. 2299, 2308, 2309

Waugh, D. W., Primeau, F., DeVries, T., and Holzer, M.: Recent changes in the ventilation of the Southern Oceans, Science, 339, 568–570, doi:10.1126/science.1225411, 2013. 2310

Whitworth, T. and Nowlin, W.: Water masses and currents of the Southern Ocean at the Greenwich Meridian, J. Geophys. Res.-Oceans, 92, 6462–6476, doi:10.1029/JC092iC06p06462, 1987. 2305, 2306

Wolf-Gladrow, D.: The expedition of the research vessel “Polarstern” to the Antarctic in 2012 (ANT-XXVIII/3), Reports on polar and marine research, 661, 2013. 2303

OSD
11, 2289–2335, 2014

Tracers in the Southern Ocean

T. Stöven et al.

Table 1. Detection limits of transient tracers. The presented values are approximate values which can deviate between different systems and the measurement conditions, e.g. lab or on board measurements.

Tracer	LOD	Unit
CFC-12	0.01	$pmol\,kg^{-1}$
SF_6	0.1	$fmol\,kg^{-1}$
^3H	0.02	TU
^3He	4.0×10^{-9}	$^3He/^4He$
^{39}Ar	8×10^{-16}	$^{39}Ar/Ar$
^{14}C	1×10^{-15}	$^{14}C/C$

OSD
11, 2289–2335, 2014

Table 2. ^{39}Ar data of the eastern Atlantic and south eastern Weddell Sea from the early 1980s. The data is taken from Rodriguez (1993).

	LAT [° N]	LON [° W]	^{39}Ar [% modern]	pressure [dBar]
Eastern Atlantic				
	40.3	−18.5	64	2700
	−5	−24	56	3400
	−0.5	−19.5	54	4100
	46	−11	49	4300
	−5	−24	46	4500
	9.5	−26	47	4600
	37.9	−17.5	39	5590
Eastern Weddell Sea				
	−61.5	−6.5	98	8
	−66.7	5	88	40
	−62.7	3	41	240
	−65.2	−2	46	245
	−61.5	−6.5	37	445
	−61.5	−6.5	44	675
	−66.7	5	34	1245
	−67.3	−0.5	38	1990
	−65.2	−2	52	3055
	−61.5	−6.5	52	4070
	−61.5	−6.5	52	4645
	−62.5	−1.2	57	5150
	−62	−1.5	56	5235

OSD
11, 2289–2335, 2014

Table 3. Constrained Δ/Γ ratios of the IG-TTD model in the northern part of the section in 1998 and 2012. The atmospheric concentration limit leads to non-constrained (n.c.) data in 2012.

	1998		2012	
Pressure [dBar]	Δ/Γ ratio	Γ [yrs]	Δ/Γ ratio	Γ [yrs]
50	0.21 (±0.48)	0 (±0)	n.c.	–
100	0.22 (±1.40)	0 (±0)	n.c.	–
150	0.74 (±0.67)	4 (±1)	n.c.	–
200	0.78 (±0.61)	5 (±2)	n.c.	–
250	0.89 (±0.72)	9 (±2)	n.c.	–
300	1.02 (±0.51)	11 (±3)	0.93 (±0.20)	9 (±1)
350	0.90 (±0.39)	12 (±3)	0.95 (±0.14)	12 (±1)
400	0.68 (±0.28)	13 (±2)	1.05 (±0.13)	15 (±1)
450	0.75 (±0.26)	14 (±2)	1.02 (±0.11)	16 (±1)
500	0.95 (±0.27)	18 (±5)	0.96 (±0.45)	17 (±5)
600	1.34 (±0.29)	32 (±8)	0.91 (±0.29)	22 (±4)
700	1.12 (±0.29)	38 (±11)	0.97 (±0.22)	34 (±8)
800	0.66 (±0.26)	33 (±11)	1.03 (±0.19)	50 (±10)
900	1.06 (±2.85)	68 (±39)	1.00 (±0.16)	71 (±16)
1000	0.53 (±1.06)	42 (±155)	0.90 (±0.12)	82 (±11)
1100	0.77 (±0.75)	77 (±50)	0.69 (±0.07)	75 (±11)
1200	–	–	0.47 (±0.08)	66 (±11)

Table A1. Mean concentrations and standard deviations of CFC-12 in the northern and southern part in 2012.

	northern part		southern part	
Pressure [dBar]	CFC-12 [ppt]	σ [± ppt]	CFC-12 [ppt]	σ [± ppt]
50	564.8	10.3	535.4	27.9
100	567.1	16.9	491.6	58.6
150	555.6	11.7	392.3	48.3
200	550.2	13.1	328.5	66.8
250	530	14.2	250	65.2
300	511.7	13.2	196.3	54.2
350	493.7	12.1	159.9	44.6
400	482.7	13.4	132.9	38.7
450	467.7	0	114.7	29
500	454.7	0	101.9	21.7
600	414.5	0	85.4	13
700	359.8	0	73.3	8
800	299.4	0	65	5.5
900	242	0	57.9	4.8
1000	197.5	1.3	52.5	5
1100	164	1.7	54.3	5
1200	130.6	2.3	51.9	4.9
1300	100.5	3.6	49.6	4.6
1400	76.6	4.9	47.8	4.4
1500	61.7	5.5	46.8	4.2
1600	54.3	4.6	46.7	4.1
1700	48.5	3.7	47.1	4.7
1800	43.9	2.9	47.8	5.8
1900	40.4	2.4	48.5	6.9
2000	37.5	2.2	49.1	7.6
2100	35.1	2.2	49.7	7.4
2200	32.8	2.3	51.2	6.4
2300	30.8	2.5	52.9	5
2400	29.3	2.8	54.6	3.8
2500	28.5	2.9	55.6	3.1
2600	28.4	2.8	55.5	3.5
2700	28.5	2.7	54.5	5
2800	28.8	2.6	53	7.1
2900	29	2.5	51.6	9.3
3000	29.3	2.4	50.8	10.8
3100	29.6	2.2	51	11.3
3200	30.1	2.2	52	11.2
3300	30.7	2.3	53.4	10.8
3400	31.3	2.5	54.9	10.5
3500	31.8	2.6	56.2	10.3
3600	33.1	2.4	57	10.4
3700	33.5	2.2	57.4	10.7
3800	34	1.7	61.2	13.1
3900	34.7	1	61	14.3
4000	35.4	0.5	–	–
4100	36.1	0.1	–	–
4200	36.9	0	–	–
4300	37.8	0.1	–	–
4400	38.8	0	–	–
4500	39.9	0.2	–	–
4600	41	0.5	–	–
4700	42.9	0	–	–

OSD
11, 2289–2335, 2014

Tracers in the Southern Ocean

T. Stöven et al.

Table A2. Mean concentrations and standard deviations of SF_6 in the northern and southern part in 2012.

	northern part		southern part	
Pressure [dBar]	SF_6 [ppt]	σ [± ppt]	SF_6 [ppt]	σ [± ppt]
50	7.3	0.2	7.9	1
100	7.3	0.2	7	1.8
150	7.1	0.3	5.9	1.8
200	6.8	0.3	3.9	1
250	6	0.5	2.8	0.9
300	5.4	0.4	2.2	0.8
350	4.9	0.3	1.7	0.7
400	4.7	0.1	1.4	0.6
450	4.5	0	1.2	0.5
500	4.3	0	1.1	0.4
600	3.6	0	1	0.4
700	2.9	0	0.9	0.4
800	2.2	0	0.7	0.4
900	1.6	0	0.7	0.4
1000	1.1	0	0.7	0.4
1100	0.8	0	0.7	0.6
1200	0.5	0	0.8	0.8
1300	0.3	0	0.9	1
1400	–	–	0.9	1.2
1500	–	–	0.9	1.3
1600	–	–	0.6	1
1700	–	–	0.6	0.9
1800	–	–	0.6	0.7
1900	–	–	0.6	0.6
2000	–	–	0.6	0.6
2100	–	–	0.6	0.6
2200	–	–	0.7	0.6
2300	–	–	0.7	0.7
2400	–	–	0.8	0.8
2500	–	–	0.8	0.8
2600	–	–	0.8	0.8
2700	–	–	0.7	0.7
2800	–	–	0.6	0.6
2900	–	–	0.5	0.4
3000	–	–	0.5	0.4
3100	–	–	0.5	0.4
3200	–	–	0.5	0.5
3300	–	–	0.6	0.6
3400	–	–	0.8	0.7
3500	–	–	0.8	0.8
3600	–	–	0.9	0.8
3700	–	–	0.9	0.5
3800	–	–	0.8	0.1
3900	–	–	0.4	0.2

OSD
11, 2289–2335, 2014

OSD
11, 2289–2335, 2014

Tracers in the Southern Ocean

T. Stöven et al.

Table A3. Mean concentrations and standard deviations of CFC-12 in the northern and southern part in 1998.

	northern part		southern part	
Pressure [dBar]	CFC-12 [ppt]	σ [± ppt]	CFC-12 [ppt]	σ [± ppt]
50	549.4	20.3	515.8	32.6
100	532.2	13.8	468.4	42.1
150	506.2	28.3	321.6	84.1
200	489	36.5	238.2	88.3
250	441.1	17.9	174	78
300	423.1	21.2	131	55.3
350	408.1	20.5	93.2	27.5
400	387.3	9.8	69.1	9.5
450	374.1	6.4	59.4	4.2
500	358.9	18.7	52.4	2
600	310.5	23	44.1	4.9
700	260.2	20.8	40.5	5.8
800	214.7	38.5	38.2	6.8
900	167.8	45	35.7	9.9
1000	122.6	40.8	33.5	12.7
1100	92.2	33.1	33	12.4
1200	68.1	24.5	32.4	11.9
1300	52.4	17.1	31.6	11.3
1400	42.3	10.5	30.7	10.6
1500	34.7	5.3	29.6	9.7
1600	28.4	3.2	28.7	8.5
1700	22.6	3.9	28.3	6.4
1800	19.1	4.1	28.4	4.1
1900	17.8	3	28.7	2.5
2000	17	2.5	28.7	2.4
2100	16.5	2.1	28.5	2.9
2200	16	1.7	30.1	1
2300	15.5	1.3	30.1	1.1
2400	15	1	30.1	1.2
2500	14.5	0.9	30.1	1.5
2600	14.2	1.1	30.1	1.9
2700	13.8	1.5	30.1	2.4
2800	13.5	1.9	30	3.2
2900	13.1	2.4	30	4.2
3000	12.7	3	30	5.4
3100	13.5	4.2	–	–

Table A4. Mean concentrations and standard deviations of SF_6 in the northern and southern part in 1998.

	northern part		southern part	
Pressure [dBar]	SF_6 [ppt]	σ [± ppt]	SF_6 [ppt]	σ [± ppt]
50	3.4	0.2	3.6	0.2
100	3.3	0.2	3.4	0.2
150	3	0.4	2.4	0.6
200	2.7	0.3	1.4	0.5
250	2.3	0.3	0.8	0.3
300	2.2	0.3	0.6	0.1
350	2	0.3	0.5	0
400	1.7	0.2	0.4	0.1
450	1.7	0.2	0.3	0.1
500	1.7	0.2	0.3	0.1
600	1.4	0.1	0.2	0
700	1.1	0.1	0.2	0
800	0.7	0.2	0.2	0.1
900	0.6	0.2	0.2	0
1000	0.3	0.1	0.2	0
1100	0.3	0.1	0.2	0
1200	0.2	0.1	0.2	0

OSD
11, 2289–2335, 2014

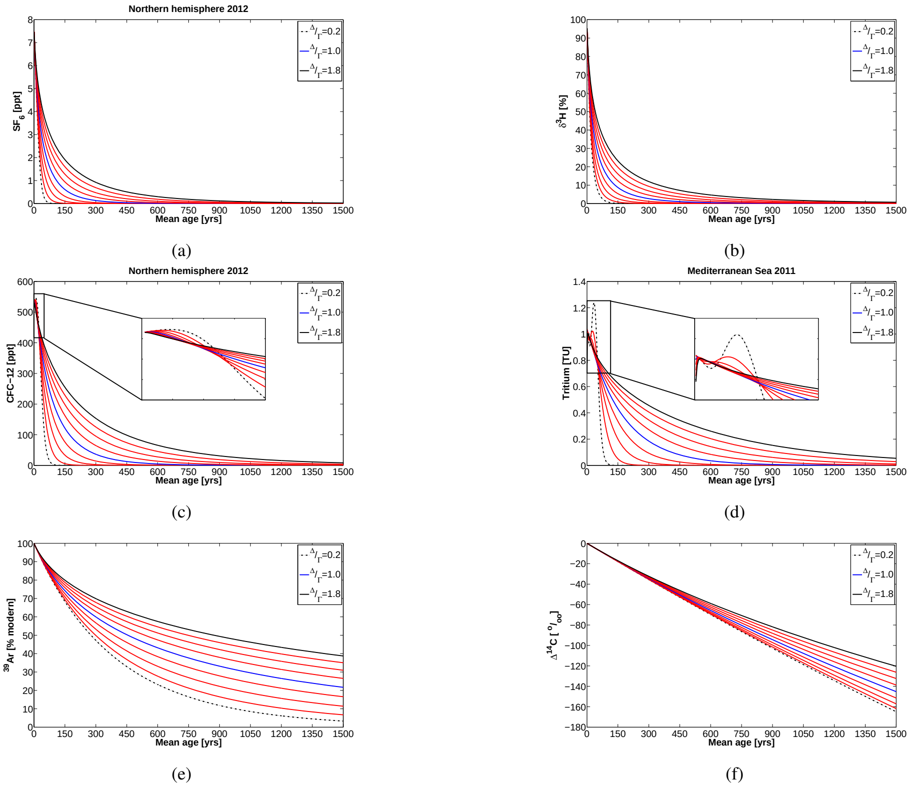

Figure 1. Transient tracer concentration of **(a)** SF_6, **(b)** δ^3H , **(c)** CFC-12, **(d)** Tritium, **(e)** ^{39}Ar, **(f)** $\Delta^{14}C$ vs. mean age for different $\Delta\,/\,\Gamma$ ratios. The standard ratio of 1.0 is shown as a blue line and the lower and upper limit as dashed and solid black line, respectively. CFC-12 and tritium show a distribution anomaly which is caused by the decreasing atmospheric concentration of both tracers. The ranges of the time scale of the transient tracers are congruent with the plot order **(a–f)** from low to high.

OSD
11, 2289–2335, 2014

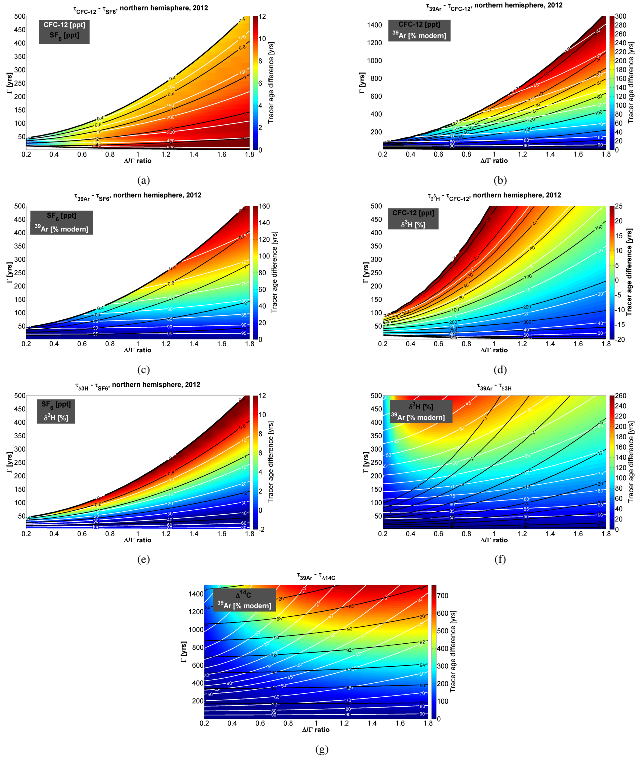

Figure 2. Validity areas of the transient tracer couples expressed with the color coded tracer age difference. The concentrations of both tracers are shown as black and white contour lines, respectively. The tracer couple and additional information are specified in the title and legend of the figures. The thick solid lines denote the analytical limits (LOD) or other restrictions such as the atmospheric concentration limit of CFC-12. The tracer couples are **(a)** CFC-12/SF_6, **(b)** CFC-12/^{39}Ar, **(c)** SF_6/^{39}Ar, **(d)** CFC-12/δ^3H, **(e)** SF_6/δ^3H, **(f)** ^{39}Ar/δ^3H, **(g)** ^{39}Ar/Δ^{14}C. The determined TAD of measured tracer data can simply be used to decide if the IG-TTD can be applied or another model is needed for further data processing.

OSD
11, 2289–2335, 2014

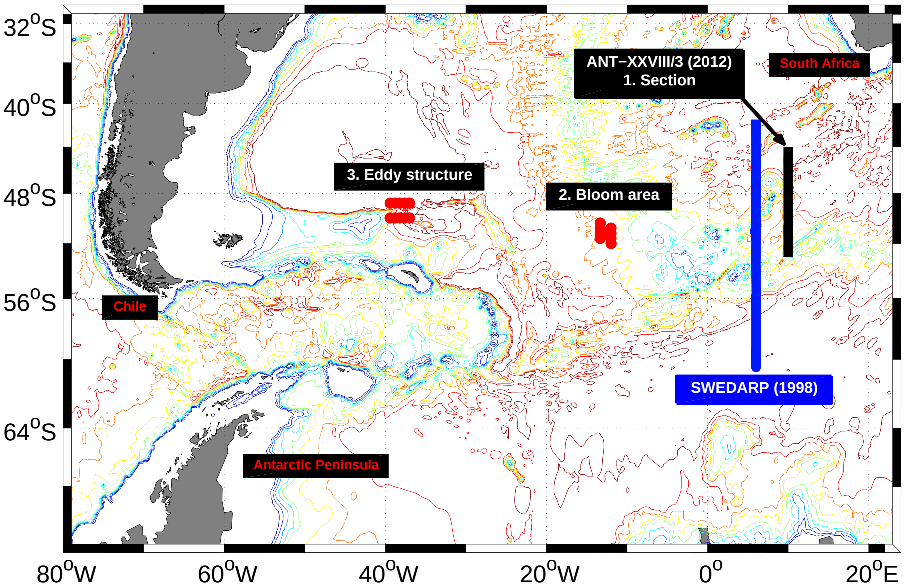

Figure 3. Transient tracer sample stations of the ANT-XXVIII/3 cruise (black and red) from Cape Town (South Africa) to Punta Arenas (Chile) in 2012. The data of the red colored bloom area (2) and eddy structure (3) are not part of this work but are available at CDIAC (see text). The section of the ANT-XXVIII/3 cruise of 2012 is highlighted as black line, the section of the SWEDARP cruise of 1998 is highlighted as blue line. The depth contours are 1000 : 500 : 5000.

OSD
11, 2289–2335, 2014

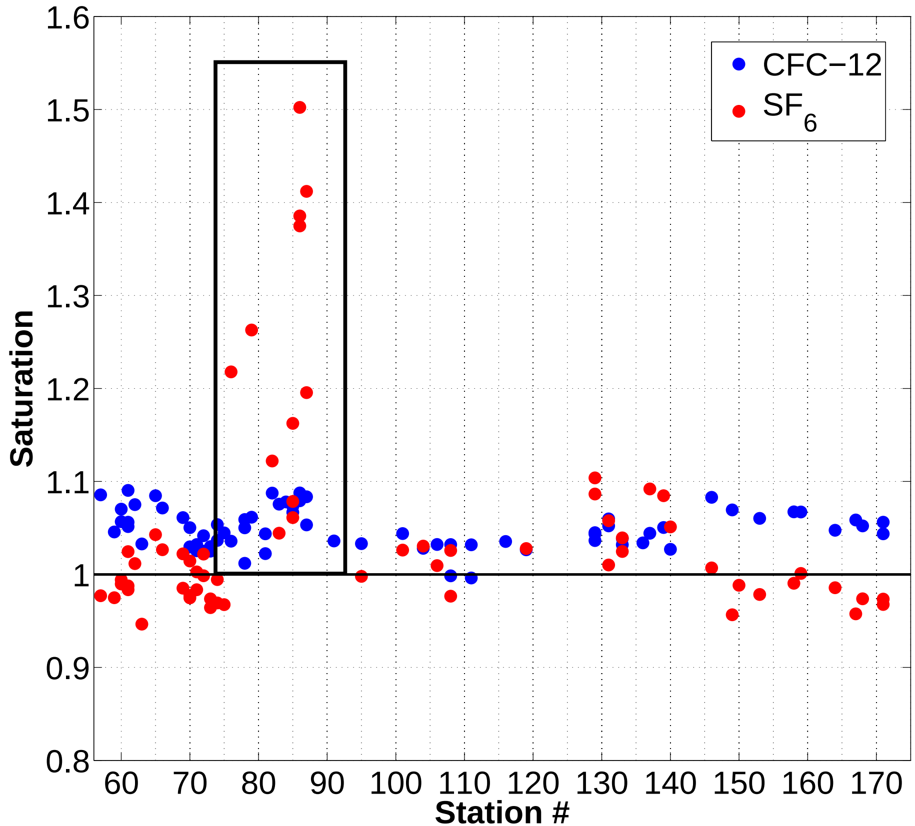

Figure 4. Surface saturation of CFC-12 (blue) and SF_6 (red) during the ANT-XXVIII/3 cruise in 2012. SF_6 shows significant supersaturation one day after heavy weather conditions with wind speeds up to force 10–11 in this area (black box).

OSD
11, 2289–2335, 2014

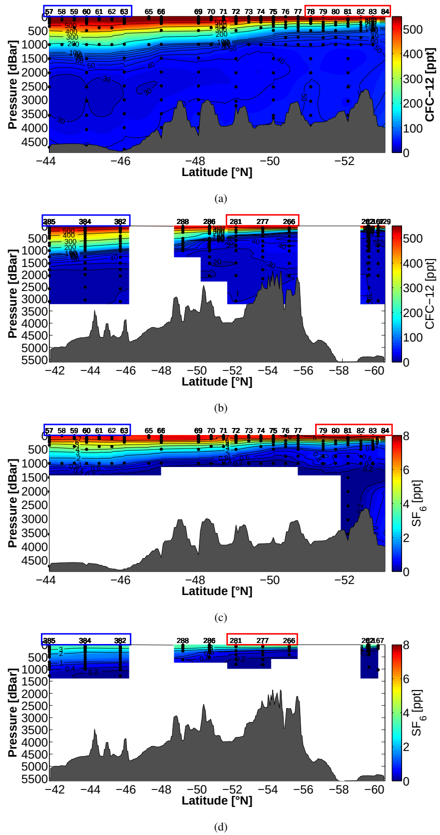

Figure 5. Southern Ocean transient tracer concentrations of **(a, b)** CFC-12 and **(c, d)** SF_6 in ppt in 1998 and 2012. Blue (SWE) and black line (ANT) in Fig. 3. Black dots indicate the sampling points.

OSD
11, 2289–2335, 2014

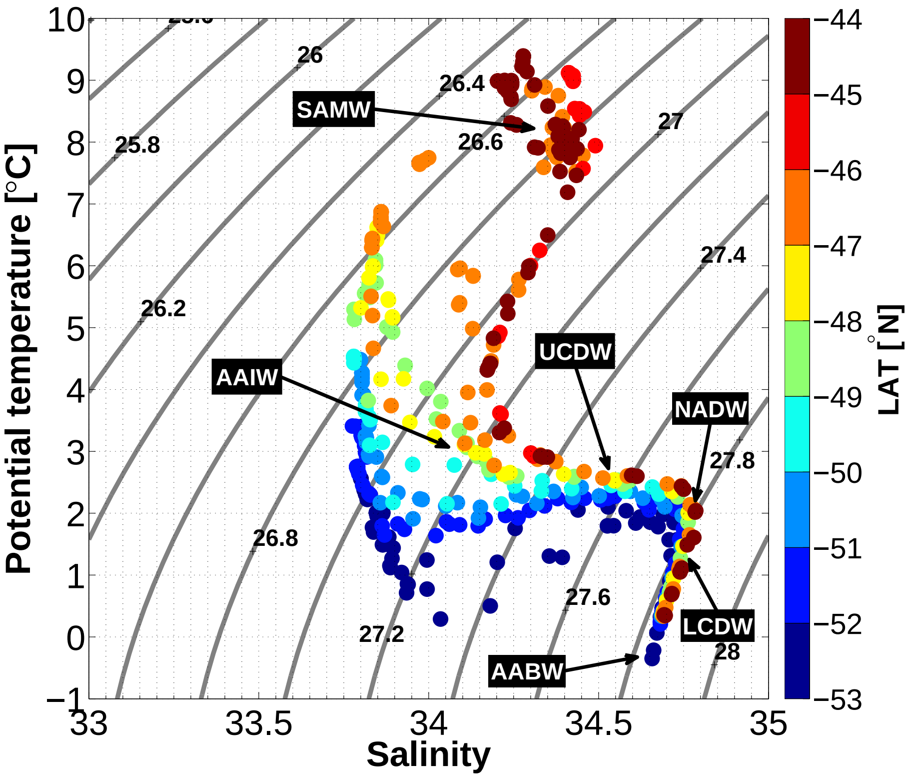

Figure 6. Plot of potential temperature vs. salinity based on the CTD bottle data. The color coding refers to the meridional position of the sample. The major water masses are highlighted, i.e. Antartic Intermediate Water (AAIW), Subantarctic Mode Water (SAMW), Upper and Lower Circumpolar Deep Water (UCDW, LCDW), North Atlantic Deep Water (NADW) and Antarctic Bottom Water (AABW).

OSD

11, 2289–2335, 2014

Tracers in the Southern Ocean

T. Stöven et al.

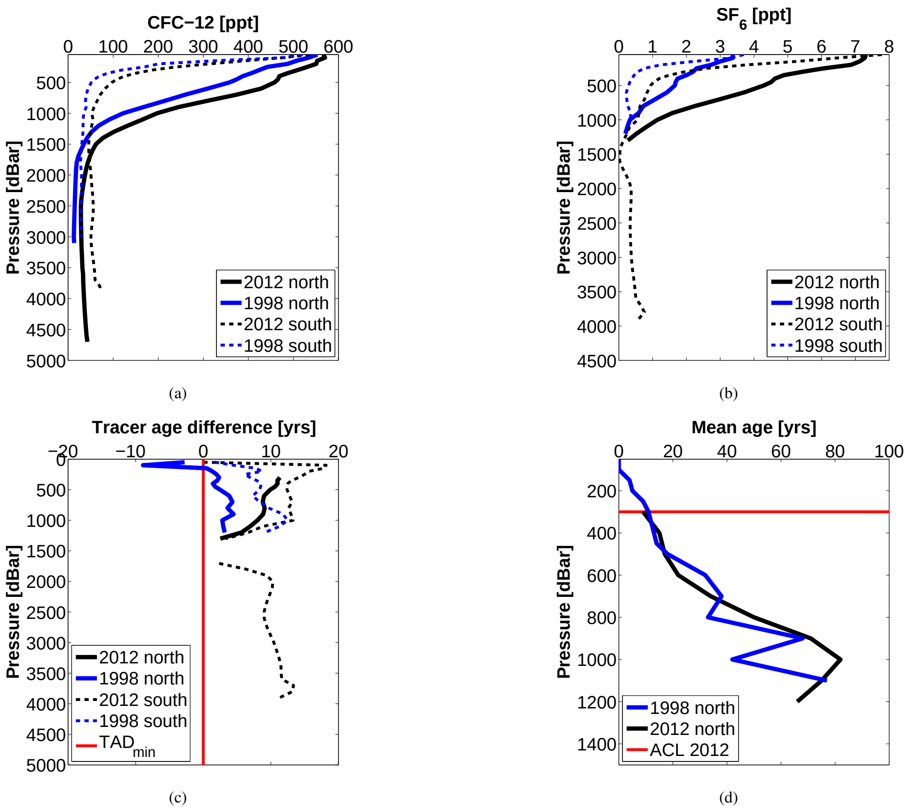

Figure 7. Interpolated profiles of **(a)** CFC-12 and **(b)** SF_6 in ppt, **(c)** the tracer age difference of CFC-12 and SF_6 and **(d)** the best mean age approach. Data of 1998 is plotted in blue and of 2012 in black, each separated in a northern part (solid lines) and southern part (dashed lines). The red line in **(d)** denotes the minimum TAD and in **(d)** the atmospheric concentration limit of CFC-12.

OSD
11, 2289–2335, 2014

Tracers in the Southern Ocean

T. Stöven et al.

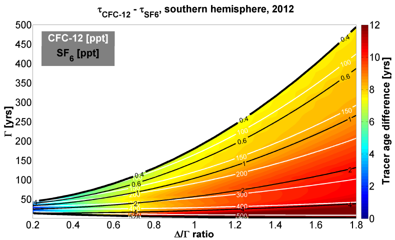

(a)

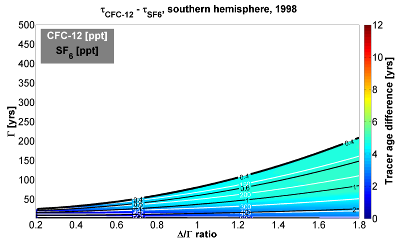

(b)

Figure 8. Validity areas of CFC-12 and SF_6 in the Southern Hemisphere for **(a)** 2012 and **(b)** 1998. The color coding of the TAD is equal for both years to highlight the time dependence of the validity area when chronological transient tracers are used. For figure explanation see caption of Fig. 2.

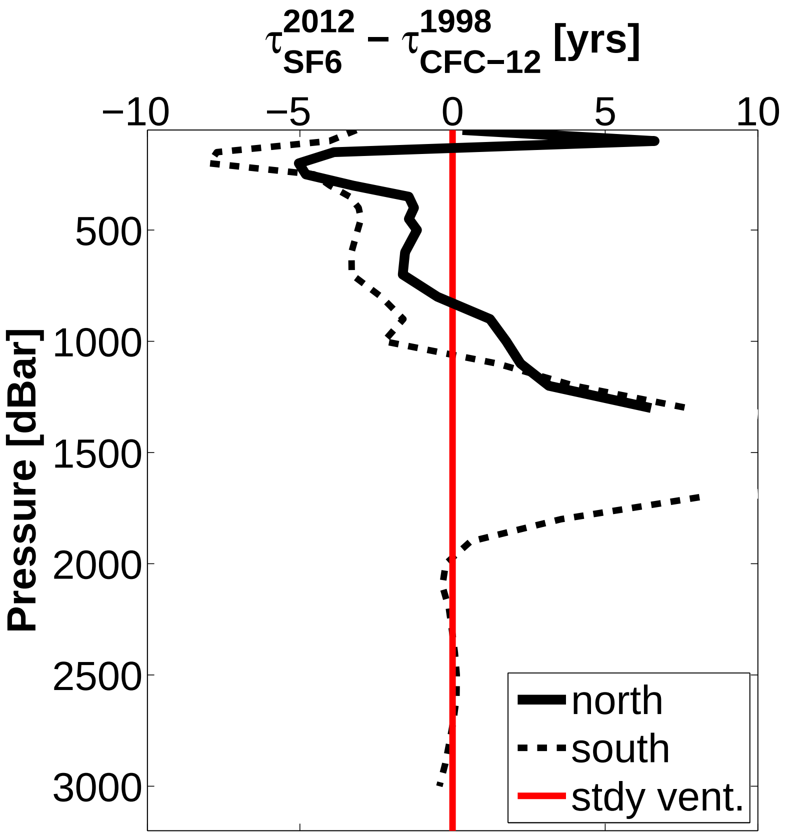

Figure 9. Time lag analysis by using the tracer age difference between CFC-12 in 1998 and SF_6 in 2012 of the northern part (solid line) and southern part (dashed line). Values above zero (red line) indicate a decreasing ventilation, values below indicate an increasing ventilation.

OSD
11, 2289–2335, 2014

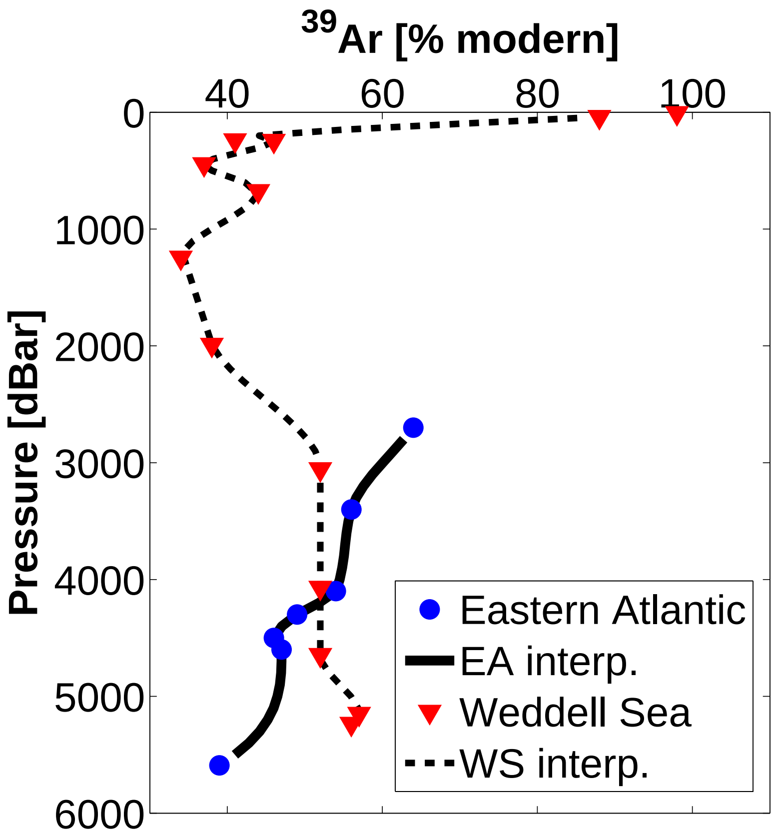

Figure 10. ^{39}Ar concentration in the eastern Atlantic (blue marker) and the south eastern Weddell Sea (red markers). The solid and dashed line refers to interpolated data points according to the depth increment of the CFC-12 and SF_6 data.

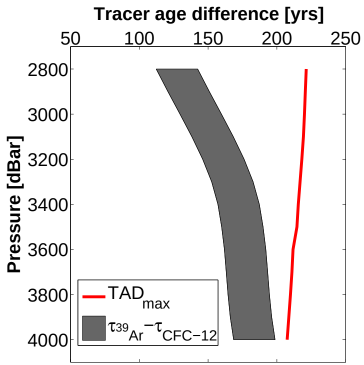

(a)

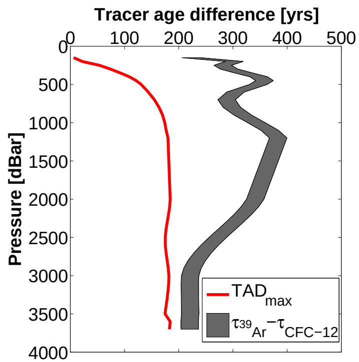

(b)

Figure 11. Theoretical TAD of CFC-12 and the estimated concentration range of ^{39}Ar (grey shaded area) of **(a)** the northern part and **(b)** the southern part. The red lines denote the maximum TAD which is the application limit of the IG-TTD.

OSD
11, 2289–2335, 2014

Tracers in the Southern Ocean

T. Stöven et al.